Australian Journal of Basic and Applied Sciences, 6(9): 1-9, 2012
ISSN 1991-8178

Design of a Differential Sensor Circuit for Biomedical Implant Applications

Sheroz Khan, Abdulwahab Deji, M., M. Mohammed Shobaki, A.H.M. Zahirul Alam, Jalel Chebil, Noreha Abdul Malik

Department of Electrical and Computer Engineering International Islamic University, Malaysia.

Abstract: This paper presents a novel approach of an inductive sensor based on the basic principle of producing inductive changes in proportion to sea saw oscillations of a horizontal bar. The circuit is supported by resistances and capacitances meant for deriving a signal from implantable devices. Basically, it's a pressure sensor which can be used for the acquisition of medical signal, and is very helpful in diagnostic procedures. Using an inductive coil sensor working on a differential manner, a physical parameter is translated into a signal with proportionate output frequency change. The results shown can be used for characterizing the materials and hence sensor with high sensitivity, linearity and responsiveness in harsh environmental condition.

Key word: Inductance-to-frequency converter, variable inductance, magnetization, pressure sensor, displacement, relative permeability.

INTRODUCTION

Accurate and real time measurement of biomedical parameters have proven pivotal in diagnosing the types and causes of illness. Such diagnostic circuits are important in order to design an intelligent control and monitoring differential device system capable of proving to be an optimal utility in the light of the fact that the use of implantable medical devices (IMDs) has been on the rise in recent past, and continues to do so in the near future. For an accurate measurement of biomedical parameter such as respiration, an efficient heart beat detector is necessary. The sensor output should be such that, disease, its causes, effect on human body and its tolerance period in the body should be determined. A pressure sensor can be made to do this medical task keeping in mind the trend, these days, of more miniature devices appearing and settling into hand gadgets bearing wireless communication utility.

Pressure sensors are broadly categorized into piezo-resistive, capacitive, Linear Variable Displacement Transducers (LVDT) and new pressure sensor (Mohammed, S.S., 2011; 2012; Ezzat, G.B., 2011). Piezo-resistive sensors are with the features of good linearity and acceptable sensitivity, but suffer from the problem of inaccuracy due to large temperature hysteresis (Ezzat, G.B., 2011; Jeevandoss, C.R., 2011). Capacitive pressure sensors exhibit features of higher sensitivity and lower temperature hysteresis, but they are usually nonlinear (Jeevandoss, C.R., 2011; Shuenn-Yuh, L., 2011; John, W.J., 2008) even in low temperature range applications. Conventional LVDT-based pressure sensors possess good linearity, highest sensitivity and lowest temperature hysteresis, but such devices have got bulky physical structures (John, W.J., 2008; Texas Instruments, 2003; Department of Physics and Astronomy, 2001). New pressure sensor is characterized with excellent linearity, high sensitivity and a low temperature hysteresis (Ezzat, G.B., 2011). This paper introduces a novel type of pressure sensor that is characterized by: a) miniature size most suited for being used in buried applications; b) excellent linearity over an arbitrary chosen pressure and displacement range; c) substantially high sensitivity; d) substantially low temperature hysteresis; e) Low power consumption; f) excellent responsiveness, and g) good level of immunity to interferences from neighboring medical devices. Each segment of this work has been put into different sections. Section I gives brief insight, section II describes the working principle, section III of this paper describes the theoretical background, derivation technique and the newest sensor circuit design. The biomedical applications of the newest pressure sensor are shown in section IV. Results from simulations and analysis are given in section V; while conclusion is presented in section VI.

I. Working Principle:

The working principle of this pressure sensor is as shown in Fig. 1 making use of a highly differential inductive mechanism. The changes in inductance are resulting from the change in the relative permeability of the movable core.

The core is made of chosen materials of different relative permeability values such as;iron, nickel and copper. The proposed sensor offers low power consumption with a change in inductance of 45.9mH over a pressure range of 0.3kPa to 12.3kPa while moving over a displacement of from 0 – 0.02m. Its sensitivity is therefore 3.73mH/kPa which is substantially high when compared to results by previously reported contemporary works on pressure sensor.

Corresponding Author: Sheroz Khan, Department of Electrical and Computer Engineering International Islamic University, Malaysia.

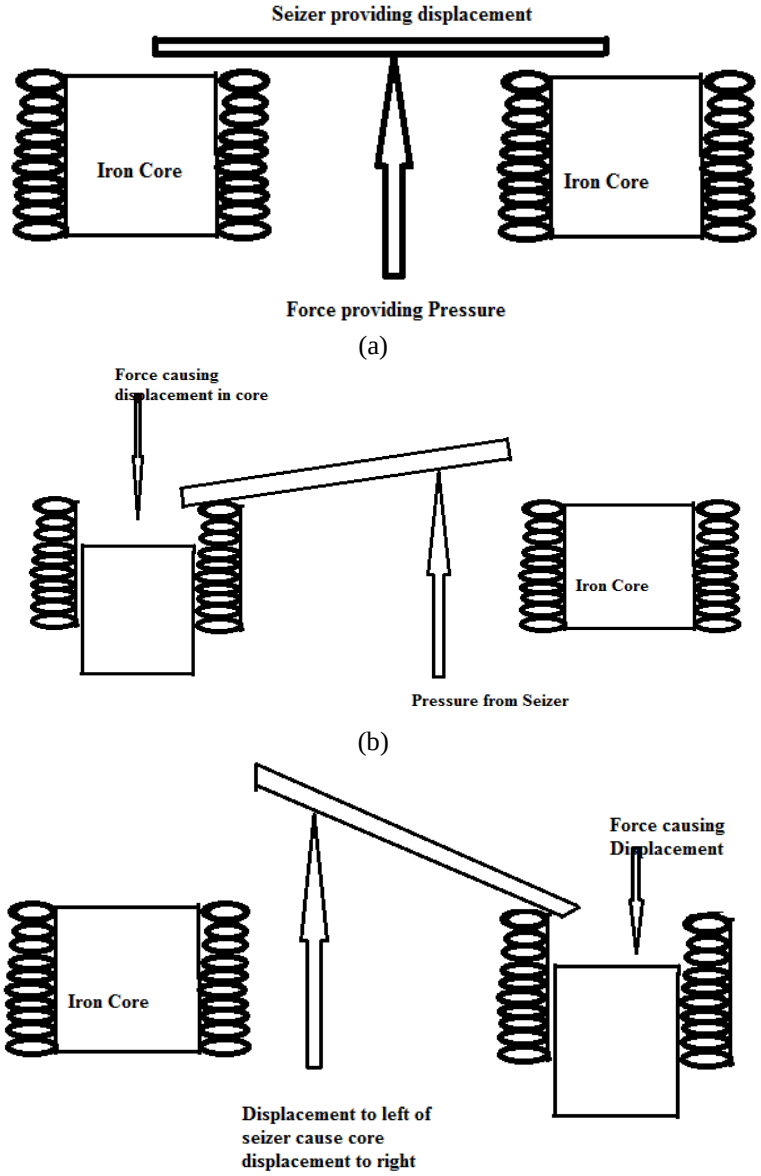

Fig. 1: (a) A conceptual design of convulsion bar resting on a pivot point moving in a sea saw manner over two magnetic coils: (b) The right bar moved down forcing the iron core on the left to be moved up. (c) The pivot bar on the left is moved down forcing the iron core on the right to be moved up.

II. Theory and Derivations:

As shown in Fig. 2 a core of known length and relative permeability is moving up and down over the entire range of the coils giving the inductance with respect to the displacement.

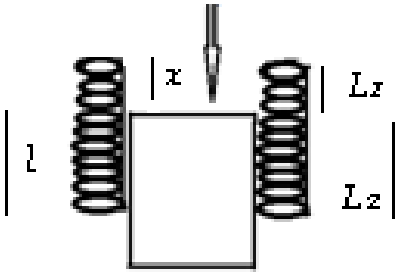

Fig. 2: Inductance splinted into two component inductive changes.

A: Inductance as a Function of Displacement of Core:

The inductance of the coil of wire is given by (Ezzat, G. B., 2011):

$$L = \frac{\mu_r \mu_0 N^2 A}{l} \quad (1)$$

Then

$$L = \frac{\mu_r \mu_0 N^2 \left(1 - \frac{x}{l}\right)^2 A}{l - x} + \frac{\mu_0 N^2 A x}{l^2}$$

$$= \frac{\mu_0 N^2 A}{l}\left(\mu_r \frac{(l-x)}{l} + \frac{x}{l}\right) \quad (2)$$

This also can be written as:

$$\boldsymbol{L = \frac{\mu_0 N^2 A}{l}\left(\frac{x}{l} + \mu_r(1 - \frac{x}{l})\right)} \quad (3)$$

Where x shows displacement by which the core move in a coil of length, l.

B: Displacement of the Core Resulting to Frequency Output:

The output frequency derived in this paper as an improvement of the previously reported work (Ezzat, G. B., 2011) is given below as:

$$f = 1.58 \frac{R}{L} \quad (4)$$

Substituting equation (3) into (4), we have;

$$\boldsymbol{f = \frac{1.58Rl^2}{\mu_0 N^2 A(\mu_r l + x(1-\mu_r))}} \quad (5)$$

C: Position of the Core as a Function of Pressure to Frequency:

The pressure caused by the force applied for moving the core is given as:

$$P_{min} = \frac{F_{min}}{A} \quad \text{Where } F_{min} = mg \quad (6)$$

The net force acting to compress the spring is given as:

$$F = kx = (P - P_{min})A \quad (7)$$

From equation (7), we displacement *x* given as

$$x = \frac{(P - P_{min})A}{k} \quad (8)$$

Substituting equation (8) into (3), we have;

$$L = \frac{\mu_0 N^2 A}{kl^2}\left(k\mu_r l + (1 - \mu_r)(P - P_{min})A\right) \quad (9)$$

Substituting equation (9) into (4), we have;

$$f = \frac{1.58\ R}{\frac{\mu_0 N^2 A}{kl^2}(k\mu_r l + (1-\mu_r)(P - P_{min})A)} \quad (10)$$

This can be arranged as:

$$\boldsymbol{f = \frac{1.58Rkl^2}{\mu_0 N^2 A(k\mu_r l + (1-\mu_r)(P - P_{min})A)}} \quad (11)$$

Detailed derivations are given in Appendix I

Circuit Design and Operation:

The conceptual structural design as presented in Fig. 2 works on the mechanism which is schematically shown in Fig. 3(a) and (b). The variation in the physical parameter such as the inductance of the coil is connected to an interface circuit (555 timer) which converts this deviation into useful frequency output as shown in equations 4 and 11.

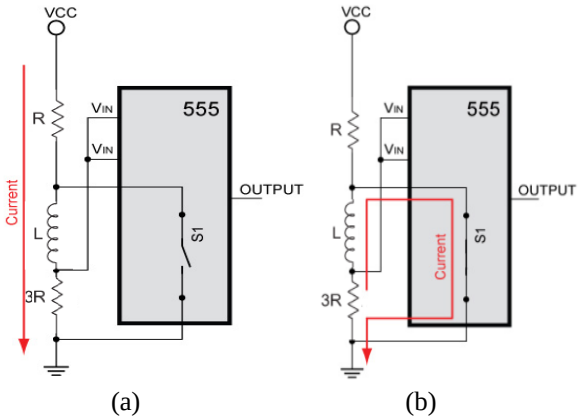

Fig. 3: The flow of current in and out and the activation of sensor interface circuit.

Here it shows how the novel pressure sensor works in transforming changes in inductance into proportionate frequency and voltage output.

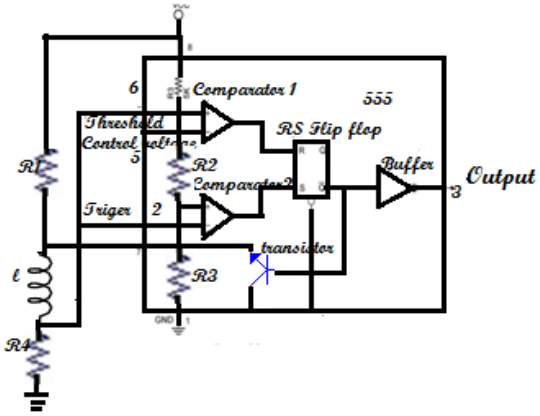

Fig. 4: Circuit Design for Converting inductance changes into relevant output.

The current and voltage waveforms from the interfaced circuit in Fig. 3 are shown in Fig. 5. The first part shows the inflow and out flow of current as it passes through the timer circuit. The vivid description is shown in Fig.4 describing the timer operation when comparator Q1 is turned on while Q2 in off mode and Q1 off when Q2 is ON.

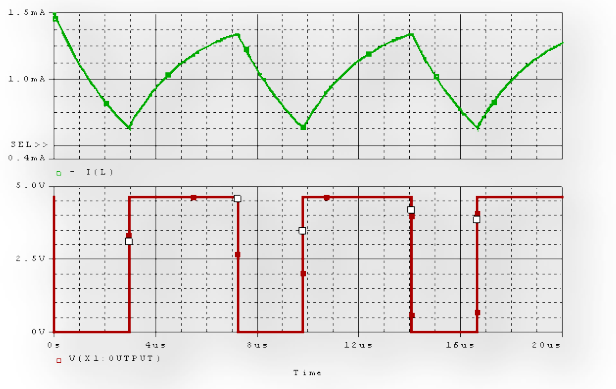

Fig. 5: Current and Voltage Response.

The iron core is inserted6mm into thecoil. The value of frequency is recorded. The core is again inserted into 12mm and then followed by 18mm, 24mm, 30mm, and 36mm respectively. When the core is fully inserted into coil, the value of the frequency is recorded. Then, the core is being pulled in 6mm steps passing over values of 6mm followed by 12mm, 18mm, 24mm, 30mm, and 36mm respectively.

When the core is being pulled out completely from the coil, the value of frequency is recorded. The above procedure is repeated three times for calculating the final results at average values. Subsequently, the same procedure is performed with core being replaced by nickel and copper, while recording the results for obtaining the result plots.

Table 1: Comparison of Sensor characteristics.

	Sensitivity	Linearity	Pre. Hyst	Tempt. Hyst
Piezor.p.s	25mV/kPa	Linear	±1% FSO	±2% FSO
Cap. Pre. Sensor	0.2nF/kPa	Nonlinear	±0.1% FSO	±0.5% FSO
LVDT	400mV/kPa	Linear	±0.5% FSO	±0.1% FSO
New Sensor	3.56mH/kPa	Linear	±0.05% FSO	±0.1% FSO
Newest Sensor	3.72mH/kPa	Highly Linear	±0.03% FSO	±0.1% FSO

The above circuit when fabricated on a chip can be fitted to a pacemaker for being applied to verify the body conditions under intense situation. In this case, the change in inductance of the coil as a function of the movement of the core respond to ambient body environment by translating the differential deviations from the sensor whose pressure or net force comes from the heart beat. This translates this implantable medical device (IMD) into signal generator. This frequency and voltage output can be modulated into a pulse stream via gatherable protocols, the application scenario is as shown in Fig.6.

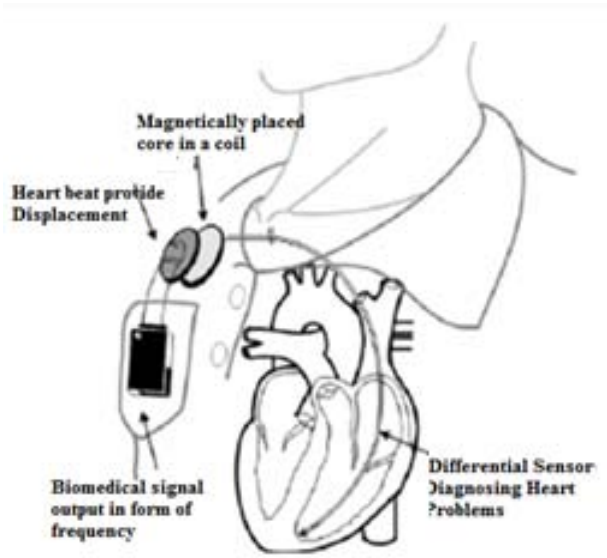

Fig. 6: Device applied to the respiratory system (Shuenn-Yuh, L., 2011).

This device comprises of coils of micro-dimensions (Imran, K., 2012; Stefanie, J., 2012) in a core interfaced with a timer in an oscillator mode. The heartbeat provides the pressure which displaces the core leading into changes in inductance produced as frequency or duty cycle output. This frequency is analyzed to show the significance of coil pressure sensor and its biomedical diagnostic applications.

Simulation Results and Analysis:

A: Basic Simulation Parameters:

For the prototype device described in this paper, here under focus are the aforementioned parameters and physical quantities.

- The length of the core and that of the coil is 20mm.
- The mass of the cores used ranges from 0.68g to 0.98g.
- The total number of turns N in the coil is 100.
- The radius of the coil is 1mm and its resistance is 1Ω, giving cross sectional area of the coil used in the simulation.
- The relative permeability of iron core is 4728, that of nickel is 600 and copper is 0.999834.

- The displacement varies from 0.001 to 0.020m. This gives a pressure range of 0.3kPa to 12.3kPa which is the dynamic range of the developed sensor, which stays in the range of pressure by heart beat.
- The spring constant, K, is 91.33N/m.
- The maximum inductance, L, obtained and the minimum was calculated $L_{min}=L_{max}/\mu_r$ for the different core material.

B: Inductive Response from the Sensor:

The change in inductance and hence in the signal output over the given range of the physical parameter is called response. This response does not remain linear over the entire range of sensing. In this case, the system presented and described in equation (3) is a differential response as shown below in Fig.7.

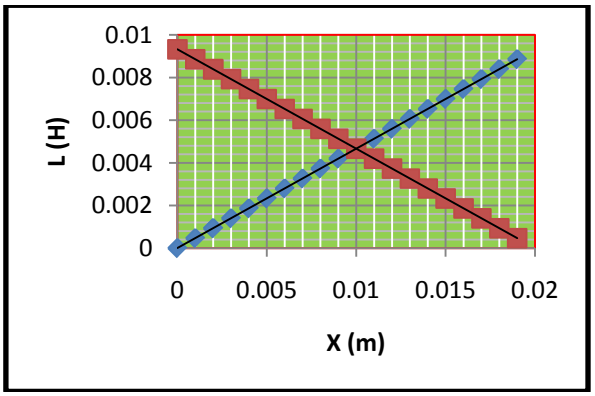

Fig. 7: Plot for Inductance L versus Displacement X.

Fig. 7 shows the total inductance of the core and its displacement as it moves in and out of the coil. This gives a symmetrical response as the breath-in and breath-out provides two-way movement replicating a differential phenomenon. A concatenation of the response is done to provide an improved linearity over a short displacement path.

B: Frequency Response from the Sensor:

From equation (5) of this paper the frequency response from the different magnetic core materials is as shown in Fig. 8.

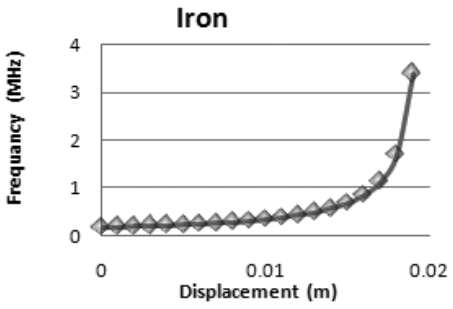

(a)

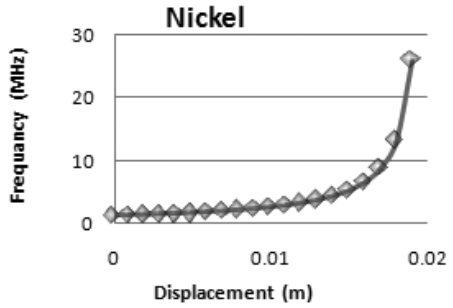

(b)

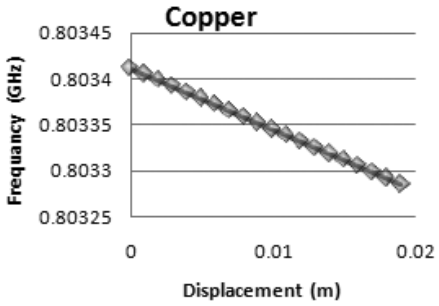

(c)

Fig. 8: (a), (b) and (c) shows frequency response for iron, nickel and copper.

The range of the output frequency is very high in paramagnetic materials (nickel) than in ferromagnetic material (iron), while there is an inverse output frequency for diamagnetic material (copper). Hence, the designed circuit is used to characterize the type of materials that could be used in some specific applications.

C: Pressure Response and Its Output Frequency:

From equation (10) of this paper, the pressure response for chosen core materials is obtained as shown in Fig. 9.

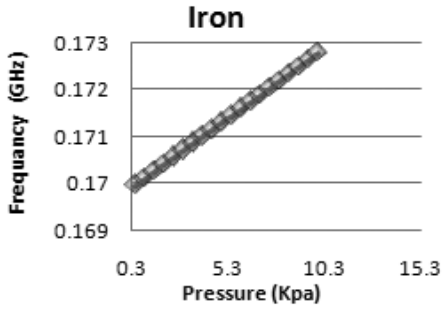

(a)

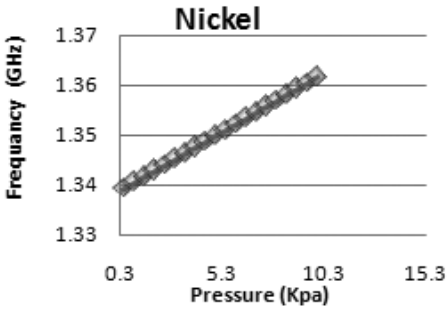

(b)

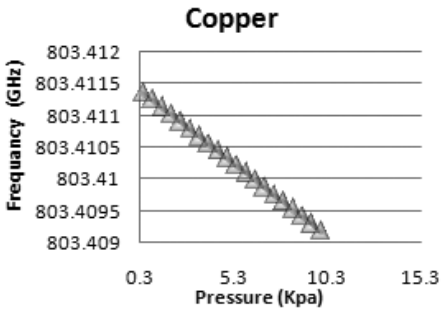

(c)

Fig. 9: (a), (b), (c):The Pressure Response of Iron, Nickel and Copper respectively.

However, as shown in Fig. 9, it is obvious that the core be made of ferromagnetic material is better than paramagnetic and diamagnetic material because it has a wider frequency range, and gives a better linearity and sensitivity compared to results in previously reported work indicated in Table 1.

Conclusion:

This paper describes a circuit which is used to convert inductance changes as a result of convulsion bar movement to frequency. The results are obtained from its application for acquisition of biomedical signal from a human body using an interface circuit properly designed for use with differential pressure sensors. In the theoretical section, the frequency response equation is derived, and then plotted in the subsequent section. In the result section, the importance of this circuit is illustrated by its an error of 0.001% of the Full Scale Operation (FSO) as shown in Table 1.The sensitivity obtained in our case is much higher than reported one in the literature and with a 0.001FSO improvement. Work on the same area is in progress trying ultimately to conform to the analytical results obtained through experimental validation.

REFERENCES

Mohammed, S.S., B. George and L. Vanajakshi, 2011. "A Magnetically Coupled Inductive Loop Sensing System for Less-lane Disciplined Traffic," in *Proc. IEEE I²MTC*, Graz, Austria, May 13–16, 2012, pp: 827-834.

Mohammed, S.S., B. George and L. Vanajakshi, 2012. "A Multiple Inductive Loop Vehicle Detection System for Heterogeneous and Lane-Less Traffic," *IEEE Transactions On Instrumentation and Measurement*, 61(5): 1353-1361.

Mohammed, S.S., B. George and L. Vanajakshi and V.J. Kumar, 2012. "A multiple loop vehicle detection system for heterogeneous and laneless traffic," in *Proc. IEEE I²MTC*, Hangzhou, China, May 10–12, 2011, pp: 1413-1417.

Ezzat, G.B. and H.M. Marvin Cheng, AUGUST 2011. "High-Sensitivity Inductive Pressure Sensor," *IEEE Transactions On Instrumentation And Measurement*, 60(8).

Jeevandoss, C.R., M. Kumaravel and V.K., Jagadeesh, 2011. "An Innovative Method for Determining the Junction Temperature of a Photovoltaic Cell" in *Proc. IEEE I²MTC*, Graz, Austria, May 13-16, 2012, pp: 1847-1850.

Jeevandoss, C.R., M. Kumaravel and V.K. Jagadeesh, 2011. "A Novel Measurement Method to Determine the *C–V* Characteristic of a Solar Photovoltaic Cell". *IEEE Trans. Instrum. Meas.*, 60(5): 1761-1767.

Shuenn-Yuh, L., C. Cheng and M.C. Liang, 2011. A Low-Power Bidirectional Telemetry Device with a Near-Field Charging Feature for a Cardiac Microstimulator. *IEEE Transactions On Biomedical Circuits And Systems*, 5(4): 357-367.

John, W.J., A.S. Raymond, 2008. "Physics for scientists and engineers with modern physics" 7th edition. Department of Physics and Astronomy, Georgia State University "Magnetic Properties of Ferromagnetic Materials table" 2001- Online at http://hyperphysics.phy-astr.gsu.edu/HBASE/Tables/magprop.html

Texas Instruments, "LM555 Data sheet" 2003.

Fan, Z., J. Holleman and B.P. Otis, AUGUST 2012. "Design of Ultra-Low Power Biopotential Amplifiers for Biosignal Acquisition Applications," IEEE TRANSACTIONS ON BIOMEDICAL CIRCUITS AND SYSTEMS, 6(4).

Stefanie, J., M. Weinzierl, I. Krause, S. Hahne, H. Rehbaum, M. Kiausch, I. Kozubek, C. Hellenbroich, M. Oertel, M. Walter, 2012. "A Multisensor Implant for Continuous Monitoring of Intracranial Pressure Dynamics," IEEE TRANSACTIONS ON BIOMEDICAL CIRCUITS AND SYSTEMS, 6(4).

Imran, K., S. Khan, O.O. Khalifa, 2012. "Wireless Transfer of Power to Low Power Implanted Biomedical Devices: Coil Design Considerations," in *Proc. IEEE I²MTC*, Hangzhou, China, Graz, Austria.

Hameed, S.A., A. Aboaba, A.A., Khalifa, O.O., Abdalla, A.H., Daoud, J.I., Saeed, R.A., Mahmoud, O., 2012. Framework for enhancement of image guided surgery: Finding area of tumor volume, Australian Journal of Basic and Applied Sciences, 6(1): 9-16. (ISI Cited publication) http://www.ajbasweb.com/

Appendix I:

Inductance of the part containing the core L_1 is given as:

$$L_1 = \frac{\mu_r \mu_0 N_1^2 A}{l-x} \text{ (A-1)}$$

The inductance of the part with no core L_2 is given as:

$$L_2 = \frac{\mu_0 N_2^2 A}{x} \text{ (A-2)}$$

The numbers of turns in the first and second inductors above the total number of the coil under consideration give by

$N = N_1 + N_2$(A-3)

And, therefore, we know that

$$\frac{N_2}{N} = \frac{x}{l} \rightarrow N_2 = \frac{Nx}{l}$$

Similarly;

$N_1 = \frac{N(l-x)}{l} = N(1 - \frac{x}{l})$ (A-4)

Substituting the values of N_1 and N_2 into equations above:

$L_1 = \frac{\mu_r \mu_0 N^2 \left(1-\frac{x}{l}\right)^2 A}{l-x} = \frac{\mu_r \mu_0 N^2 A(l-x)}{l^2}$(A-5)

$L_2 = \frac{\mu_0 N^2 \left(\frac{x}{l}\right)^2 A}{x} = \frac{\mu_0 N^2 A x}{l^2}$(A-6)

The total inductance is the series sum of the individual inductances L_1 and L_2, given as:

$L = L_1 + L_2$ (A-7)